# A New Tracking System for Three Magnetic Objectives

Wan'an Yang[1,2,3,4], Chao Hu[2], Mao Li[2], Max Q.-H. Meng[2,5], and Shuang Song[2]

[1]Shenzhen Institute of Advanced Integration Technology, Chinese Academy of Sciences/The Chinese University of Hong Kong, Shenzhen Institutes of Advanced Technology, CAS, Shenzhen, Guangdong 518067, China,
[2]Institute of Computing Technology, Chinese Academy of Sciences
[3]Graduate School of the Chinese Academy of Sciences
[4]Department of Computer and Information Technology, Yi Bin University, Sichuan 644000,China,
[5]Department of Electronic Engineering, Chinese University of Hong Kong, Shatin, N.T., Hong Kong

**We have implemented a new noninvasive multiobjective tracking system, which can be used for localization of an endoscope and monitoring of heart valve prostheses and gastrointestinal transit of solid oral dosage forms or nutrients. The marker is modeled as a magnetic dipole, and the magnetic field at some point is regarded as summation of those from three dipoles. By minimizing the squared errors of magnetic field values between measurements and calculation using a hybrid of the particle swarm optimization (PSO) algorithm and the clone algorithm, an iterative result can be obtained, which is taken as the initial guess of the Levenberg-Marquardt (L-M) optimization method, and the first point can be determined. Subsequently, the previous computed point is used as the next initial guess of L-M algorithm, and the successive points are calculated. The tracking results demonstrate that the average position error for three objectives is 3.7 mm and the average orientation error is 1.8° when the objectives move randomly in the space surrounded by the sensor array.**

***Index Terms*—Dipole, hybrid algorithm of PSO and clone scheme, L-M algorithm, magnetic marker, multiobjective tracking, sensor array.**

## I. Introduction

RECENTLY, many researchers have proposed magnetic localization and orientation technique in human medical applications [1]–[7]. For instance, Schlageter *et al.* built a system to track a permanent magnet with five degrees of freedom by using a 2-D array of Hall sensors [7]. C. Hu *et al.* have built up a localization and orientation system for wireless capsule endoscope [8]. J. A. Baldoni and B. B. Yellen have developed a magnetic tracking system for monitoring the performance and activity of mechanical heart valve prostheses [9]. Similarly, J. Wang *et al.* devised a magnetic localization system to track 3-D tongue movements during speech and ingestion [10]. The technique uses a magnet as the objective that can generate a static magnetic signal without power supply, which makes it easy to build a wireless tracking system with less invasion for long-term monitoring of internal objects. The human body has the magnetic permeability very close to air (air relative permeability $= 1.0000004$) [11], so it exerts very little influence on the static magnetic signal such that it is possible to achieve high tracking accuracy (about 3 mm when tracking a single magnetic objective) [4], [5], [7], [8].

In the previous research, the proposed tracking systems can only trace or localize one single magnetic objective. However, there are a lot of cases that should localize and track multiple objectives in practical applications, such as magnetic drug tracking, the navigation of medical instruments, and multiobjective tracking in virtual reality, entertainment, training, etc. Take localization for a wireless capsule endoscope as an example: the localization error might be caused by respiration or motion of the body when localizing the endoscope inside the gastrointestinal tract by using a single objective tracking system. While in a three-objective tracking system, it is possible to obtain localization parameters of the endoscope inside the body and magnetic objectives outside the body at the same time, so the position parameters of the endoscope inside the body can be accurately determined with respect to magnetic objectives outside the body. This relative localization approach can greatly decrease the negative effect of the movement of the human body, and there is not much increase in the hardware cost.

The organization of this paper is as follows. In Section II, we present the mathematical model of magnetic field produced by dipole and the coordinate system for magnet's location. In Section III, we introduce the method and hardware of the tracking system, and in Section IV, we propose the localization and orientation algorithm. In Section V, we present the tracking results related to the localization and orientation accuracy and the track of three objectives, which is followed by the conclusions in Section VI.

## II. Mathematical Model of Magnet's Field

A well-known approximation for the field produced by a magnet whose largest dimension is much smaller than the distance from the observer is that of a point dipole. Fig. 1 shows a cylindrical magnet with length $L$, radius $\delta$, and uniform magnetization $M_0$ ($1.032 \times 10^6$ A/m for our Nd-Fe-B magnets with size of $\Phi 5$ mm $\times$ $L12$ mm). Let $\mathbf{X}_l = (x_l - a, y_l - b, z_l - c)^T$ be the vector that represents a spatial point $s = (x_l, y_l, z_l)^T$ with respect to the magnet position $(a, b, c)^T$. The magnetic flux density at s can be calculated as [4]:

$$\mathbf{B}_l = B_T \left( \frac{3(\mathbf{H}_0 \cdot \mathbf{X}_l)\mathbf{X}_l}{R_l^5} - \frac{\mathbf{H}_0}{R_l^3} \right) \quad (1)$$

Manuscript received November 03, 2009; revised January 18, 2010 and April 11, 2010; accepted August 25, 2010. Date of publication September 16, 2010; date of current version November 30, 2010. Corresponding author: C. Hu (e-mail: chao.hu@siat.ac.cn).

Color versions of one or more of the figures in this paper are available online at http://ieeexplore.ieee.org.

Digital Object Identifier 10.1109/TMAG.2010.2076823

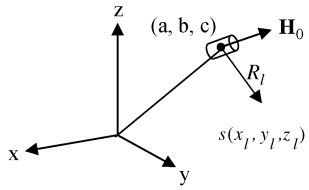


Fig. 1. Coordinate system for magnet's location.

where $B_T = \mu_r\mu_0\delta^2 LM_0/4$; $\mu_r$ is the relative permeability of the medium (in the air, $\mu_r \approx 1$); $\mu_0$ is the magnetic permeability of the air ($4\pi \times 10^{-7}$ T $\cdot$ m/A); $R_l = \sqrt{(x_l-a)^2+(y_l-b)^2+(z_l-c)^2}$; and $\mathbf{H}_0 = (m,n,p)^T$ is the normalized vector representing the direction of the magnet's magnetism.

Assume that there are $N$ sensors, with the $l$th sensor located at $(x_l, y_l, z_l)^T$, $1 \le l \le N$, and assume that there are $M$ dipoles. If the distance between any two dipoles is 10 times larger than the largest dimension of the magnet, the magnetic flux density at point $s$ can be regarded as the linear superposition of that generated by every dipole. In (1), we assume that the radius of the magnet dipole is small enough so that two surfaces of the dipole can be considered as point sources. One concern is the error induced by this assumption, and it is proved that the error induced by the approximation is related to $1/(\sqrt{1+(\delta/R)^2})$, where $R$ is the distance between the center of magnet and evaluation point [11]. (if $R$ is 10 times larger than $\delta$, the error will be smaller than 0.51%). The magnetic flux density at the $l$th sensor location can be represented by (2) [4]

$$\mathbf{B}_l = B_{lx}\mathbf{i} + B_{ly}\mathbf{j} + B_{lz}\mathbf{k} \quad (l = 1, 2, \cdots, N) \tag{2}$$

where $\mathbf{i}$, $\mathbf{j}$, and $\mathbf{k}$ are unit vectors along x-axis, y-axis, and z-axis respectively; $B_{lx}$, $B_{ly}$, and $B_{lz}$ are orthogonal components as shown in (3)–(5) at the bottom of the page, where $R_{lq} = \sqrt{(x_l-a_q)^2+(y_l-b_q)^2+(z_l-c_q)^2}$, and $q$ represents the $q$th dipole (tiny magnet). Because the $q$th magnet's orientation $(m_q, n_q, p_q)^T$ can be determined by two-dimensional parameters, we add the following constraint:

$$m_q^2 + n_q^2 + p_q^2 = 1. \tag{6}$$

In the following experiment, because the magnets are manufactured by the same materials and have the same dimension, we regard that the parameter $B_{T_q}$ in (3)–(5) has the same value. With enough sensor data $(B_{lx}, B_{ly}, B_{lz})$, parameters $(a_q, b_q, c_q, m_q, n_q, p_q)$ can be computed by using special optimization algorithms according to (3)–(6). There are five independent parameters for each magnet, so tracking $M$ isolated magnets would require $5M$ 1-axis sensors at least. However, the accuracy would be improved with more sensors [7].

## III. Material and Methods

The hardware of the tracking system is shown in Fig. 2, including a magnetic sensor array, amplifier and control circuit, a power supply, a personal computer (PC), and an analog-to-digital converter (ADC).

Because each magnet objective has five localization parameters, the minimum sensor number is 5 for each magnet objective, or two three-axis magnetic sensors. The more the sensors, the higher the accuracy [7], [2]. However, through the simulation experiment, as shown in Fig. 3, we find that the localization accuracy increases sharply with 4, 6, 8, 12, or 16 three-axis sensors distributed on 0.5 m $\times$ 0.5 m square plane uniformly; however when the three-axis sensor number is larger than 16, the localization accuracy improves little. In order to obtain 3 mm or better localization accuracy with the magnet in size of $\Phi 5$ mm $\times L12$ mm moving in the 0.5 m $\times$ 0.5 m $\times$ 0.5 m sensing space, we build a cubic (four planes) sensor array and each plane is composed of 16 sensors, so the system is composed of 64 sensors. The real experimental results show the system is satisfactory with the accuracy of 3 mm.

Three cylindrical magnets with size of $\Phi 5$ mm $\times$ $L12$ mm are utilized as magnetic objectives. The Honeywell magnetic sensor, HMC1043, is 3-axis anisotropic (ARM), which has a range $\pm 6 \times 10^{-4}$ T and a resolution $1.2 \times 10^{-8}$ T. Each sensor is connected to successive amplification and processing circuit. The sensor has four resistors made by thin films on the silicon base working in a differential mode. When the input magnetic intensity changes, there is differential resistance variation in the four resistors, and a linear voltage will be outputted by Wheat-stone bridge. Subsequently, an amplification circuit amplifies this voltage output by using the instrumentation amplifiers (AD623). The amplified analog data is obtained by analog-to-digital (A/D) converter and further processed by the computer. In the experiment, to meet the approximate condition of (1), (2), the magnetic flux density should be measured under the condition that the ratio $(d/r_1)$ between the largest dimension $(d)$ of the magnet and the distance $(r_1)$ from the

$$B_{lx} = \sum_{q=1}^{M} B_{T_q}\left\{\frac{3\left[m_q(x_l-a_q)+n_q(y_l-b_q)+p_q(z_l-c_q)\right](x_l-a_q)}{R_{lq}^5} - \frac{m_q}{R_{lq}^3}\right\} \tag{3}$$

$$B_{ly} = \sum_{q=1}^{M} B_{Tq}\left\{\frac{3\left[m_q(x_l-a_q)+n_q(y_l-b_q)+p_q(z_l-c_q)\right](y_l-b_q)}{R_{lq}^5} - \frac{n_q}{R_{lq}^3}\right\} \tag{4}$$

$$B_{lz} = \sum_{q=1}^{M} B_{Tq}\left\{\frac{3\left[m_q(x_l-a_q)+n_q(y_l-b_q)+p_q(z_l-c_q)\right](z_l-c_q)}{R_{lq}^5} - \frac{p_q}{R_{lq}^3}\right\} \tag{5}$$

magnet to the point of field evaluation is smaller than 0.1, and that the ratio $(d/r_2)$ between the largest dimension $(d)$ of the magnet and range interval $(r_2)$ of any two magnets is also smaller than 0.1.

In the real sensor array system, the sensitivity, position, and orientation of different sensors are not identical, so we should calibrate these parameters of all sensors [12], [13]. Once these sensor parameters are correctly determined, the accuracy can be improved. Fig. 4 shows the average location error for locating single objective before and after calibration. The average location error after calibration decrease 1.4 mm.

The magnetic flux density used in computing the magnet's location and orientation is that produced only by three magnets, not including the earth's magnetic field. However, in the tracking process, the measured magnetic signals in the magnetic sensors are the summations of those of the magnets and the earth. In order to filter the earth's magnetic field, the system records the earth's magnetic field in the initiation process of the system, and the data of the earth's magnetic field are subtracted when sensor data are sampled during tracking. In the tracking process, if the earth's magnetic field and environmental magnetic field fluctuate, the experimental results would be affected. If more accurate results are required, the experiment should be conducted in the shield room. Another method is to use the 3-axis magnetic sensor to measure the fluctuations in the earth's magnetic field, then all the sensor data deduct these fluctuations.

In both calibration procedure and location error evaluation, the predetermined position and orientation of the cylindrical magnet should be read. In order to implement it, the organic planes used for fastening the sensors and the test-shelf are uniformly divide into marked intervals in 5 mm. For reading the location and orientation coordinates conveniently, we put the magnet to the place where the two scale marks intersect in some specific orientations such as $(m = 1, n = 0, p = 0)$, $(m = 0, n = 1, p = 0)$, and $(m = 0, n = 0, p = 1)$. Because the length and radius of the cylindrical magnet are known, the center of the magnet is consequently determined.

## IV. Tracking Algorithm

It is possible to implement real-time tracking $M$ independent magnetic objectives at the same time according to (2)–(5) (e.g., $M \geq 2$), and the unknown parameters to be solved are 6 times of $M$. The number of the local optimal solution increases as unknown parameters increase. The algorithm such as Newton-Gauss method or L-M scheme is easy to converge to local optimal solution for inverse estimation of so many parameters in nonlinear systems (3)–(6). In order to implement tracking three cylindrical magnets in $0.5\ \text{m} \times 0.5\ \text{m} \times 0.5\ \text{m}$ space, we have to find out an improved optimization algorithm. In the following performance evaluation of improved algorithm, the main hardware configurations of computer are listed as following: CPU: P4 2.4 GHz, memory: 1 GB, and the software is VC++6.0.

### A. The Definition of Objective Function

Equations (3)–(6) are high-order nonlinear equations, and one possible approach to solve these equations is to apply nonlinear optimization methods. In (7)–(9), shown at the bottom of the page, we define error functions as follow to evaluate the performance of the algorithm.

$(B_{lx}, B_{ly}, B_{lz})$ represent the measured data of the sensors. The total objective error is the summation of the above three errors:

$$E = \overline{E}_x + \overline{E}_y + \overline{E}_z. \tag{10}$$

This is the least square error problem, by minimizing the objective error $E$ through an appropriate algorithm, the position and orientation parameters of the magnetic field sources can be determined. Note that the 3-axis sensor number $N$ should be equal to or larger than 5 in order to determine the value of 18 unknown parameters for tracking three magnetic objectives.

### B. Choosing the Localization Algorithm

There are many nonlinear optimization algorithms, such as the directed search method, Newton-Gauss method, Powell method, and L-M algorithm. These algorithms are characterized by high time efficiency, but the disadvantage is that the initial guess must be given for the algorithm, if the initial guess is far from the true solution, the iterative result is not likely correct because they are usually locally convergent. In the multiobjective tracking system, it is very difficult to give initial position and orientation guess that close to the solution because the tiny magnets can locate any unknown positions and orientations in the space of sensor array. Another difficulty is that the other algorithm consume so much time that the system cannot implement real-time tracking for magnetic objectives. We must find a method that can overcome the two difficulties.

$$\overline{E}_X = \sum_{l=1}^{N} \left\{ B_{lx} - \sum_{q=1}^{M} B_{Tq} \left\{ \frac{3\left[m_q(x_l - a_q) + n_q(y_l - b_q) + p_q(z_l - c_q)\right](x_l - a_q)}{R_{lq}^5} - \frac{m_q}{R_{lq}^3} \right\} \right\}^2 \tag{7}$$

$$\overline{E}_Y = \sum_{l=1}^{N} \left\{ B_{ly} - \sum_{q=1}^{M} B_{Tq} \left\{ \frac{3\left[m_q(x_l - a_q) + n_q(y_l - b_q) + p_q(z_l - c_q)\right](y_l - b_q)}{R_{lq}^5} - \frac{n_q}{R_{lq}^3} \right\} \right\}^2 \tag{8}$$

$$\overline{E}_Z = \sum_{l=1}^{N} \left\{ B_{lz} - \sum_{q=1}^{M} B_{Tq} \left\{ \frac{3\left[m_q(x_l - a_q) + n_q(y_l - b_q) + p_q(z_l - c_q)\right](z_l - c_q)}{R_{lq}^5} - \frac{p_q}{R_{lq}^3} \right\} \right\}^2 \tag{9}$$

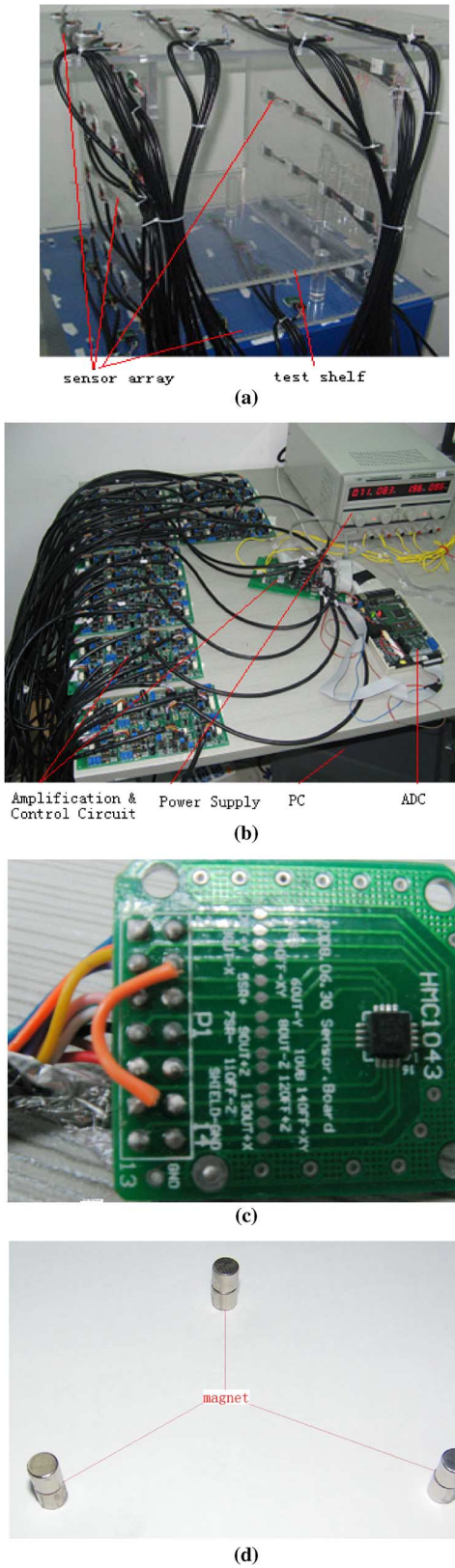


Fig. 2. Hardware of the tracking system: (a) sensor array, test shelf; (b) amplification & control circuit, power supply, ADC; (c) HMC1043 PCB circuit; (d) magnet.

### C. Particle Swarm Optimization (PSO) Algorithm

Follow Eberhart and Kennedy's naming conventions. Let $D$ be the dimension of the solution space. Assume that $n$ is the population size, the $i$th particle is $\mathrm{x}_i = (x_{i1}, x_{i2}, \ldots, x_{iD})$ $(1 \le i \le n)$. We also assume that the previous best position of the $i$th particle is $\mathrm{P}_i = (p_{i1}, p_{i2}, \ldots, p_{iD})$; the index of the best position of particle in the whole group is $g$, and the flight velocity is $\Delta\mathrm{x}_i = (\Delta x_{i1}, \Delta x_{i2}, \ldots, \Delta x_{iD})$. For each evolution, all the particles update themselves with the following two equations:

$$\Delta x_{id}(t+1) = w \times \Delta x_{id}(t) + c_1 \times r_1 \times (p_{id}(t) - x_{id}(t)) + c_2 \times r_2 \times (p_{gd}(t) - x_{id}(t)) \quad (11)$$

$$x_{id}(t+1) = x_{id}(t) + \Delta x_{id}(t+1). \quad (12)$$

Here, $c_1$, $c_2$ are known as acceleration constants, adjusting the weight of single particle's experience and group particles' experiences, and $w$ is inertia weight constant, and $r_1$ and $r_2$ are random numbers in the interval [0, 1]. The fitness function for PSO algorithm is total object error $E$ defined by (7)–(10).

The parameters $c_1$, $c_2$, and $w$ have influence on the convergence and execution time, especially for the parameter $w$. The larger the value of $w$ is, the slower the algorithm converges, but the easier the algorithm finds global minimum. Contrarily, the smaller the value of $w$ is, the faster the algorithm converges, but the more difficult the algorithm finds global minimum. Usually, the value of $w$ is selected between 0.2 and 0.8, and $w$ is taken

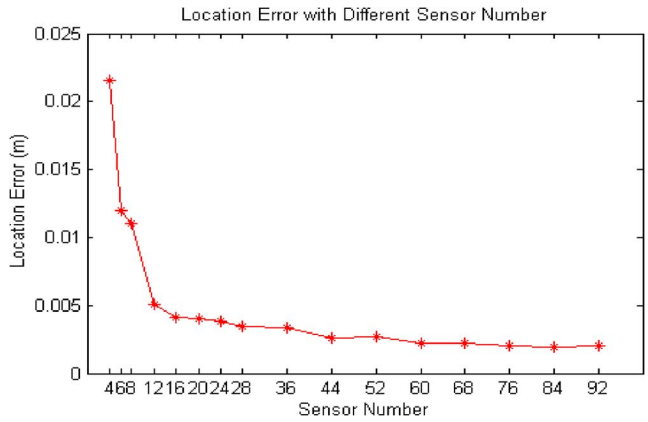


Fig. 3. Localization error with different sensors.

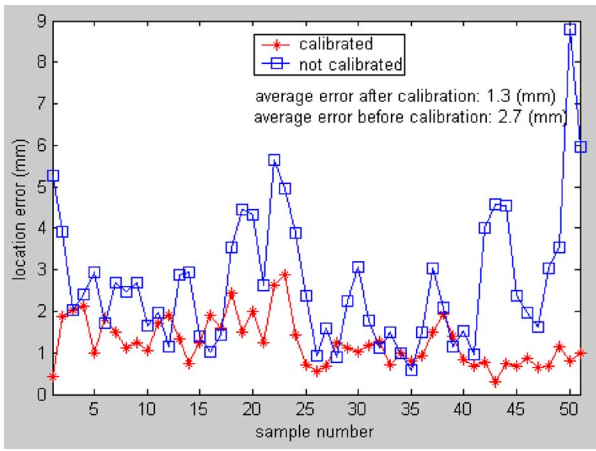


Fig. 4. Comparison of average location errors before and after calibration.

TABLE I
FAILURE RATIO BY PSO ALGORITHM

| No. | 1 | 2 | 3 | 4 | 5 | 6 | 7 | 8 | 9 | 10 |
|---|---|---|---|---|---|---|---|---|---|---|
| divergence number/40 computations | 8 | 6 | 7 | 6 | 7 | 4 | 10 | 4 | 6 | 7 |

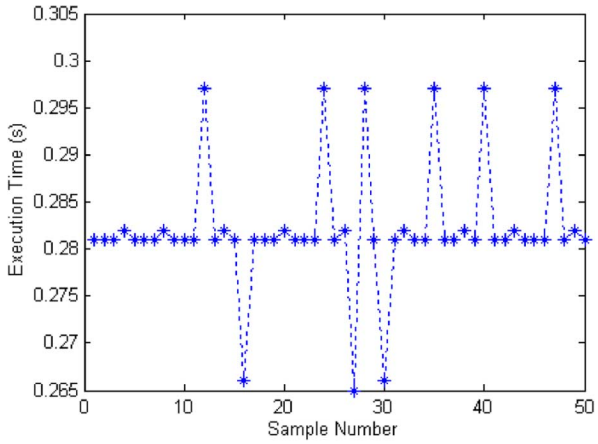


Fig. 5. Execution time of PSO algorithm.

as 0.7298 [14] at the first step of iteration, then it is deduced according to $w(\mathrm{t}+1) = 0.2 \times w(\mathrm{t})$ ($t$ represents iteration number). We let $c_1$, $c_2$ be 2 [14], [15]. However, the parameters $c_1$, $c_2$, and $w$ are assigned different values in different references, and the best values of the parameters need further study.

The merit of the PSO algorithm is that the initial guess is not required to search for the solution; as long as we give the ranges of all unknown parameters and initialize particles in the ranges of the parameters, an iterative solution can be obtained. Of course, the other types of evolutionary-strategy algorithms, such as genetic algorithm, might have the same advantage. However, in our previous research [17], we find that the PSO algorithm outperforms the genetic algorithm when searching for the solution of complicated high-order nonlinear equations in the tracking magnetic objective task, so we choose the PSO algorithm. In the iteration process, the boundaries of magnet's position parameters are length, width, and height of the space surrounded by the sensor array, and the orientation parameters are confined within $[-1, 1]$ according to (6). For the computing, the population size and maximum iteration number are set at 150 and 70, respectively. We measured the divergence ratio and execution time of the PSO algorithm, and the results are shown in Table I and in Fig. 5, respectively. The divergence probability is about 16.3%, and the average execution time is about 0.282 s.

Although the PSO algorithm can give a desirable solution in most cases, its convergent probability is too low. In the localizing process, the $B_T$ for each objective in (1) can be measured in advance, if so, 18 parameters should be determined. Alternatively, the $B_T$ of each objective can also be regarded as an unknown parameter for searching; in this case, 21 parameters should be determined, so many parameters are very liable to cause the divergence of the algorithm. So we proposed the hybrid algorithm to decrease divergence probability.

### *D. The Hybrid Algorithm of PSO and Clone Algorithm*

The PSO algorithm has a specific direction, and the particles always move towards the individual and group's best location. Once the particle falls into local extremum, it is quite difficult for the particle to jump out of it. The clone algorithm can enhance the local search by producing a new subgroup whose population size is proportional to the fitness of the particle, and maintain diversity by initializing the particles whose fitness levels are very low. In the iteration process of clone algorithm, the particles can not share information between each other because they evolve according their random mutation. In order to utilize the advantages of PSO and clone algorithms, we introduce evolution equation of PSO algorithm into the clone algorithm. Because the particles have already utilized their previous individual optimization information in the clone algorithm, we only take global optimization information into account in the PSO algorithm. Thus, in the hybrid algorithm, all the particles update themselves with (13) and (12) [16]

$$\Delta x_{id}(t+1) = w \times \Delta x_{id}(t) + c \times r \times (p_{gd}(t) - x_{id}(t)). \quad (13)$$

The process of hybrid algorithm is as follows.

1) Initialize a population, including particle's original position and flight velocity.
2) Compute all the particles' fitness according to (7)–(10).
3) Check whether the algorithm should be stopped.
4) Update all the particles according to (12) and (13).
5) Put $k$ particles with best fitness into group $Am$.
6) Produce new clone group $Ac$ by cloning every particle of group $Am$, and the clone number $n_c$ of every particle is inverse-proportional to its fitness. (Here, it is a minimization problem. If it is a maximization problem, the clone number is proportional to particle's fitness).
7) Mutate every particle from $Ac$, (the mutation ratio $\beta$ is inverse-proportional to its fitness).
8) Compute every particle's fitness in clone group $Ac$ according to (7)–(10).
9) If there exists a particle $p_c$ from $Ac$ which parent is $p_r$, ($f(p_c) < f(p_r)$, $f$ is objective function), substitute $p_c$ for $p_r$, and update global optimization particle $p_g$.
10) Return to step 3).

In step 6), the clone number $n_c$ is computed by (14)

$$n_c = \left[\frac{\alpha\, n}{i}\right], \quad i = 1, 2, \ldots, n \quad (14)$$

where $\alpha$ is known as clone constant whose value is in (0, 1), and $n$ is population size; $i$ is the sequence number of the particle (the particles are sorted regarding their objective function value, smallest to biggest).

In the evolution, to guarantee the particles with lower fitness have lower mutation probability (this is a minimum problem; if it is a maximum problem, the particles with lower fitness have

TABLE II
FAILURE RATIO BY HYBRID ALGORITHM

| No. | 1 | 2 | 3 | 4 | 5 | 6 | 7 | 8 | 9 | 10 |
|---|---|---|---|---|---|---|---|---|---|---|
| Divergence number/40 computations | 1 | 1 | 2 | 3 | 0 | 1 | 2 | 2 | 2 | 1 |

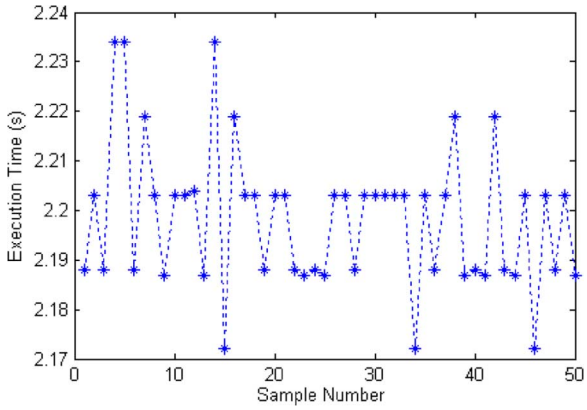


Fig. 6. Execution time of hybrid algorithm.

higher mutation probability), and to keep diversity of the particles, we adopt a self-adapted mutation operator as shown in (15) and (16) [16]

$$\Delta x_{id}=\Delta x_{id}+\beta\times(0,1),\quad 1\le d\le D,\quad 1\le i\le n \tag{15}$$

$$\beta=f(\mathbf{x}_i)\Big/\sum_{j=1}^{n} f(\mathbf{x}_j) \tag{16}$$

where $N$ (0, 1) is a random number obeying the law of standardized norm distribution.

We also investigate the execution time and the divergence probability of the hybrid algorithm. The failure ratio are shown in Table II, and the divergence probability is about 3.8% according to Table II. Fig. 6 shows the execution time of the hybrid algorithm, and the average time is about 2.198 s.

### *E. The Final Tracking Algorithm*

In the evolution, every particle searches for a probable solution in its neighborhood, so the hybrid algorithm is not only characterized by the global convergence that PSO algorithm has, but it also has the advantage of searching for the local optimal solution that the clone algorithm has. If iterative results of the hybrid algorithm and the L-M algorithm are globally convergent, the accuracy of the solutions can both meet the need of localization. So we can obtain a solution only by the hybrid algorithm; however, the average time consumed by the hybrid algorithm is about 2.198 s, which is too long to meet the need of real-time tracking for objectives, and the time consumed by L-M algorithm is about 0.2 s, which completely meets the need of real-time tracking. But an initial guess is necessary for the L-M algorithm; the result of the hybrid algorithm can just be considered as the initial guess. The probability that the hybrid algorithm converges to the global minimum is much higher than the PSO algorithm does, but it is still low. In order to guarantee high convergence probability, we let the hybrid algorithm search for the solutions for three times continuously, and choose the best one (which has minimum fitness) as the initial guess of the L-M algorithm, whose result is served as the first point of the magnet's track. In the subsequent tracking, the previous computed point is regarded as the initial guess of the L-M algorithm in every computation, whose result is taken as the new point of the magnets' track. For the divergence probability of the hybrid algorithm is about 3.8%, the divergence probability that the hybrid algorithm is divergent for three times consecutively is smaller than 0.006% (as long as one of three computations is convergent, we can take it as initial guess of L-M algorithm), the time for computing the first point is about 6.6 s. (If the hybrid algorithm search for the solutions for two times continuously, the divergence probability for two times consecutively increases to 0.14%, and the time searching for the first point decreases to 4.4 s. Certainly, you can choose four or more times of iterations to obtain high convergence probability, but more time is consumed). Using this tracking method, we can guarantee that the first point can be found with probability 99.9%; because the last computed point is very close to the predetermined value of the computing point, the iteration process of L-M algorithm is convergent.

## V. TRACKING RESULTS

In order to evaluate the performance of the three-objective tracking system, we define the position error $E_p$ and orientation error $E_o$ as follows:

$$E_p=\frac{1}{3}\sum_{i=1}^{3}\sqrt{(a_{ic}-a_{it})^2+(b_{ic}-b_{it})^2+(c_{ic}-c_{it})^2} \tag{17}$$

$$E_o=\frac{1}{3}\sum_{i=1}^{3}\sqrt{(m_{ic}-m_{it})^2+(n_{ic}-n_{it})^2+(p_{ic}-p_{it})^2} \tag{18}$$

where $(a_{ic}, b_{ic}, c_{ic}, m_{ic}, n_{ic}, p_{ic})$ represent the calculated position and orientation parameters, and $(a_{it}, b_{it}, c_{it}, m_{it}, n_{it}, p_{it})$ represent predetermined position and orientation parameters of the $i$th magnet, the orientation can also be represented by angle, calculated by $2\sin^{-1}(E_o/2)$.

Tracking experiments are carried out in a normally unshielded room. The position and orientation errors are calculated when the three magnets randomly placed as long as the distance between the magnets and between the sensor and magnet meet the constraint (see Sections II and III). As shown in Figs. 7 and 8, the average position error is about 3.7 mm, and the average orientation error is about 1.8°. Fig. 9 shows the real-time track of the three magnets.

## VI. DISCUSSION AND CONCLUSION

A real-time tracking system for multiple magnetic objectives is implemented. The magnetic fields produced by multiple tiny permanent magnets can be regarded as the overlap of the fields of the dipoles, which is a reasonable approximation since that the ratio $(d/r_1)$ between the largest dimension $(d)$ of the magnet and the distance $(r_1)$ from the magnet to the point of field evaluation is smaller than 0.1, and since that the ratio $(d/r_2)$ between

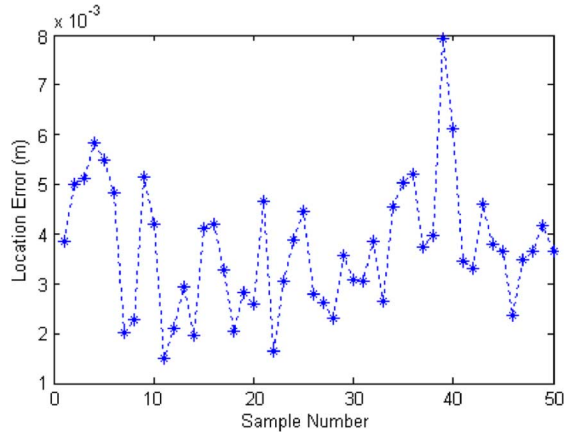


Fig. 7. Position errors.

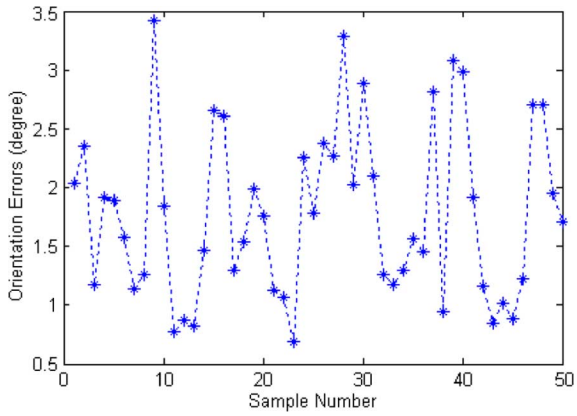


Fig. 8. Orientation errors.

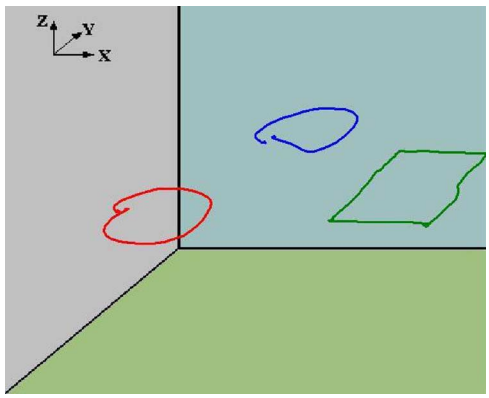


Fig. 9. The real-time track of three magnets.

the largest dimension $(d)$ of the magnet and range interval $(r_2)$ between any two magnets is also smaller than 0.1. Compared with the localization and orientation system of single magnetic objective [8], the position error rises by 1.7 mm, and orientation error rises by 0.2°. However, the sensing space for three objectives is $0.5\ \mathrm{m} \times 0.5\ \mathrm{m} \times 0.5\ \mathrm{m}$. It is much larger than in which the single objective moves randomly. The localization and orientation errors are mainly caused by noise and model error. In the future, we plan to reduce position and orientation error by improving the SNR of the sensor signals and decreasing model error; meanwhile, we need to study localization and orientation for more objectives.

## ACKNOWLEDGMENT

This work was supported by grants from Key Lab of Robotics & Intelligent System, Guangdong Province (2009A060800016), the Guangdong/CAS Cooperation Project (2009B091300160), National Natural Science Foundation of China (60904031), Shenzhen Science & Technology Research Funds, the Knowledge Innovation Engineering Funds of CAS, and the Funds of SRF for ROCS, SEM.

## REFERENCES

[1] C. Hu, M. Q.-H. Meng, and M. Mandal, "Efficient magnetic localization and orientation technique for capsule endoscopy," *Int. J. Inf. Acquisition*, vol. 2, no. 1, pp. 23–36, 2005.

[2] C. Hu, M. Q.-H. Meng, and M. Mandal, "A linear algorithm for tracing magnet's position and orientation by using 3-axis magnetic sensors," *IEEE Trans. Magn.*, vol. 43, no. 12, pp. 4096–4101, Dec. 2007.

[3] M. Q.-H. Meng, T. Mei, J. Pu, C. Hu, X. Wang, and Y. Chan, "Wireless robotic capsule endoscopy: State-of-the-art and challenges," in *Proc. 5th World Congr. Intelligent Control and Automation*, Jun. 15–19, 2004, pp. 5561–5565.

[4] X. Wang, M. Q.-H. Meng, and Y. Chan, "A low-cost tracking method based on magnetic marker for capsule endoscope," in *Proc. Int. Conf. Information Acquisition*, Jun. 21–25, 2004, pp. 524–526.

[5] N. M. Prakash and F. A. Spelman, "Localization of a magnetic marker for GI motility studies: An in vitro feasibility study," in *Proc. 19th Annu. Int. Conf. IEEE on Engineering in Medicine and Biology Society*, Oct. 30–Nov. 2, 1997, vol. 6, pp. 2394–2397.

[6] X. Chen, S. Tamura, D. Lin, and Y. Du, "A 3D localization and navigation method for endoscope by magnetic field," *J. Comput. Res. Develop.*, vol. 39, no. 2, 2002.

[7] V. Schlageter, P.-A. Besse, R. S. Popovic, and P. Kucera, "Tracking system with five degrees of freedom using a 2D-array of Hall sensors and a permanent magnet," *Sens. Actuators A: Phys.*, vol. 92, no. 1, pp. 37–42, 2001.

[8] C. Hu, W. Yang, D. Chen, M. Q.-H. Meng, and H. Dai, "An improved magnetic localization and orientation algorithm for wireless capsule endoscope," in *Proc. 30th Annu. Int. IEEE EMBS Conf.*, Vancouver, BC, Canada, Aug. 20–24, 2008, pp. 2055–2058.

[9] J. A. Baldoni and B. B. Yellen, "Magnetic tracking system: Monitoring heart valve prostheses," *IEEE Trans. Magn.*, vol. 43, no. 6, pp. 2430–2432, Jun. 2007.

[10] J. Wang, X. Huo, and M. Ghovanloo, "A quadratic particle swarm optimization method for magnetic tracking of tongue motion in speech disorders," in *Proc. 30th Annu. Int. IEEE EMBS Conf.*, Vancouver, BC, Canada, Aug. 20–24, 2008, pp. 4222–4225.

[11] C. Hu, "Localization and orientation system for robotic wireless capsule endoscope," Univ. Alberta, 2006, pp. 16–42.

[12] C. Hu, Q.-H. Meng, and M. Mandal, "The calibration of 3-axis magnetic sensor array system for tracking wireless capsule endoscope," in *Proc. IEEE Int. Conf. Intelligent Robots and Systems*, Beijing, China, 2006, pp. 162–167.

[13] A. Plotkin, V. Kucher, and Y. Horen *et al.*, "A new calibration procedure for magnetic tracking systems," *IEEE Trans. Magn.*, vol. 44, no. 11, pp. 4525–4528, Nov. 2008.

[14] H. Guo, X. Jin, and X. Hu, "Research on the solving of nonlinear equation group based on swarm particle optimization," *Comput. Eng. Appl.*, vol. 42, no. 15, pp. 72–74, 2006.

[15] Z. Ren, Y. San, and J. Chen, "Improved particle swarm optimization and its application research in tuning of PID parameters," *J. Syst. Sim.*, vol. 18, no. 10, pp. 2870–2873, 2006.

[16] L. Liu, Z. Cai, and J. Tang, "Immunity clone algorithm with particle swarm optimization," *Comput. Appl.*, vol. 26, no. 4, pp. 886–887, 2006.

[17] W. Yang, C. Hu, M. Q.-H. Meng, S. Song, and H. Dai, "A six-dimensional magnetic localization algorithm for a rectangular magnet objective based on a particle swarm optimizer," *IEEE Trans. Magn.*, vol. 45, no. 8, pp. 3092–3099, Aug. 2009.